Positron annihilation spectroscopic studies of sintering effect on sol–gel-synthesized SiO_2 wide band gap semiconductor nanocrystals

Anjan Das

Department of Physics, A.P.C. Roy Government College, Siliguri, Darjeeling 734 010, India

Sol–gel procedure followed by sintering was used to prepare silica nanoparticles. Their structural properties were examined using XRD and HRTEM. Estimation of band gap and characterization of various type of defects were carried out by UV-Vis spectroscopy and positron annihilation spectroscopy. Though bulk SiO_2 is an insulator, calculated band gap was in the range of wide band gap semiconductor region. High value of positron lifetime indicated presence of void type defects on sintering in air. The defect profile has changed from unsintered samples. Coincidence Doppler broadening spectroscopy revealed the momentum characteristics of core as well as valence electrons.

Keywords: Band gap, defects, positron annihilation spectroscopy, sol–gel procedure, silica nanoparticles.

CERAMIC nanoparticles are being studied presently for their improved electrical, chemical and magnetic properties over their bulk counterparts. Advancement in synthesis procedure has helped in the production of nanosized silica, SiO_2, which is being widely used as a filler in engineering composites, as an additive in rubber and plastic. SiO_2 is applied suitably for insulation as its heat capacity and melting point are low. Various methods are used to synthesize silica nanoparticles such as sol–gel process, flame synthesis[1] and reverse microemulsion. By adopting sol–gel process one can produce uniformly crystallized oxide nanocrystallites. It is necessary to adopt the sol–gel process to prepare silica nanoparticles. Bulk silica is an insulator, although it can alter its energy level distribution in its nanophase specially after sintering. Ultraviolet and visible (UV–Vis) light absorption spectroscopy is used to determine the optical band gap of the samples[2]. Structural defects like vacancies and their complexes have important roles in tailoring the properties of the semiconductor nanocrystalline materials. It is rarely found in literature, the dynamics and interaction of defects in silica nanoparticles at various stages of the experimental sequence. Although sintering effect can change many properties in semiconductor oxide nanoparticles, it is necessary to study the behaviour of electrical properties, particularly the defect structure of silica nanoparticles. Hassan[3] studied silica bulk materials on third component of positron lifetimes only. Little attention has been paid to the sintered and unsintered comparison of silica nanoparticles. Positron annihilation spectroscopy (PAS) is a unique, nondestructive tool for the characterization of defects in oxide semiconductor nanoparticles. In this work, we use PAS to gather information on defects and variations of the different positron annihilation parameters that have been monitored with the changes in synthesis environment.

e-mail: anjadas@gmail.com

Experimental details

Synthesis of SiO_2 nanocrystallites

To synthesize the sintered and unsintered SiO_2 nanoparticles by sol–gel method, we used sodium silicate solution with pH value of 11.1–11.6 as the precursor. The solution contained 7.0–8.0% Na_2O and 25.0–28.0% SiO_2. Ammonium hydroxide solution of 33% extra pure and ethanol, analytical grade, were used in this preparation. At first a mixture of ammonia and ethanol was prepared by taking equal amounts, i.e. 200 ml of each. Next 20 ml of sodium silicate solution was added to 100 ml distilled water and this precursor was added dropwise to the ammonia–ethanol mixture. The resulting mixture was centrifuged and washed with distilled water after ageing for 1 h and finally dried at 600°C when a white powder was obtained. The whole process was repeated to prepare two more samples. One of the samples was sintered in air. For this, the sample in powder form was dispersed in distilled water in a 50 : 50 wt% ratio. Slips were poured in a plastic frame of 10×20 mm^2 set on plaster moulds, and then dried to make green compacts. Air pressure was 10^5 Pa: $p(O_2) = 2 \times 10^4$ Pa and the heating rate was 15°C/min. The sample was kept isothermally at 1100°C for 3 h and then cooled in the furnace. The other two samples were annealed at 1100°C and 1200°C respectively.

Structural characterization and UV–Vis measurements

The samples were examined by X-ray diffraction (XRD) technique (Bruker D8 Advance diffractometer) with

CuKα ($\lambda = 1.5406$ Å) X-ray radiation at 40 kV and 40 mA. All the three samples were scanned from 10° to 50° with a scanning speed of 2° (2θ) per minute. Further, the morphology and shape of the sample particles were studied by high-resolution transmission electron microscopy (HRTEM). The microscope used (FEI Model Tecnai S-twin) had a resolution 0.24 nm. Optical absorption measurements (UV–Vis; with a Perkin-Elmer UV–Vis-NIR spectrophotometer) (Lambda 750) were performed by dissolving requisite amounts of the nanoparticulate samples in hydrochloric acid.

Positron annihilation measurements

To carry out the positron annihilation measurements, a 10 μCi strong ^{22}Na source was deposited in solution form on a very thin (~2 mg cm^{-2}) Ni foil. After drying and folding the foil it was kept immersed in a column of the powdered sample taken in a glass tube. Vacuum pump was used to continuously evacuate the glass tube to remove traces of air and moisture between the crystallites. The sample covered the source in larger thicknesses than the penetration range of the positrons emitted from the source. The positrons annihilated within the sample materials only. A gamma–gamma coincidence set-up was used to record the positron lifetime spectra employing barium fluoride (BaF_2) scintillators coupled to photo multiplier tubes (XP2020Q), and the associated electronic arrangements for pulse processing and storage. The set-up was measured for its time resolution (full width at half-maximum). For this, the coincident gamma-rays from a ^{60}Co source under the ^{22}Na experimental range of energy signals were used. The time resolution was as low as 170 ps. To measure the coincidence Doppler broadening (CDB) of annihilated gamma rays, two high pure germanium (HPGe) detectors of energy resolution 1.27 and 1.33 keV respectively, at 0.511 MeV were used. A large number of counts (more than 10^6 in positron lifetime and about 10^7 in CDB spectra) were acquired within reasonable time by accurate calibration of the channels. The computer programs PALSfit[4] and LAMS[5] were used to analyse the spectra.

Results and discussion

X-ray diffraction studies

Figure 1 presents the XRD spectra of some of the samples. The observed peaks of diffracted X-rays match with the standard values (JCPDS no. 86-1565). All the samples exhibited the main peaks corresponding to (100), (011), (110) and (102) planes of the hexagonal structure. Any secondary phases were not observed in the spectra of any of the samples. This indicates that the synthesized samples are highly pure. The lattice constant of synthesized SiO_2 nanoparticles varied a little. Further, the mean crystallite size of the different samples for spherical shape were estimated from the Debye–Scherrer equation[6]

$$d_c = \frac{0.9\lambda}{\beta \cos\theta}, \tag{1}$$

where β indicates the full width at half maximum of the diffraction peak corresponding to an angle θ and λ is the wavelength used for the measurement. The most intense peak (011) in the XRD patterns has been used to find out the average crystallite size and their values are 33.3 nm (1100°C), 46 nm (1200°C) and 55.4 nm (sintered at 1100°C). Each spectrum was used to estimate the lattice constants (a) of corresponding samples. The Bragg's equation was combined with the plane spacing (d) to get the relation

$$\frac{4\sin^2\theta}{\lambda^2} = \frac{1}{d^2} = \frac{4}{3}\frac{h^2 + hk + k^2}{a^2} + \frac{l^2}{c^2}, \tag{2}$$

Equation (2) can be rewritten as $\sin^2\theta = X(h^2 + hk + k^2) + Yl^2$, where $X = \lambda^2/3a^2$ and $Y = \lambda^2/4c^2$. As hkl is always an integer, the measured $\sin^2\theta$ values are divided by 3, 4, 7, etc. and the results tabulated. The lowest common quotient is found out from the table and corresponding $\sin^2\theta$ values are divided by this results will be some integers which are $h^2 + l^2 + k^2$. The possible value of X is obtained

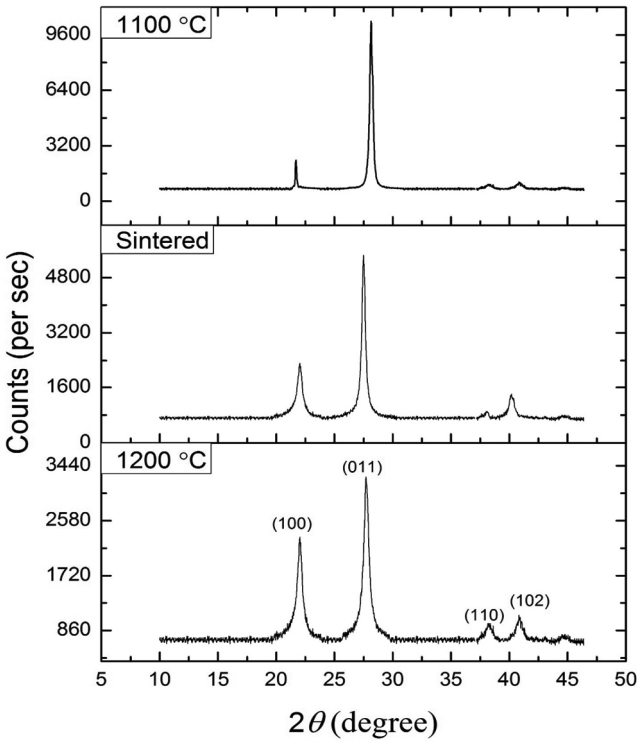

Figure 1. XRD spectra of the synthesized SiO_2 nanocrystalline samples.

for diffraction peaks corresponding to *hk0* with $l = 0$. The value of X obtained in this process can satisfy the following relationship for general indices h, k, and l: $Yl^2 = \sin^2\theta - X(h^2 + hk + k^2)$. From this equation Y can be obtained. From the values of X and Y, the values of a and c can be obtained.

Figure 2 shows the variation of lattice constant, estimated from the above procedure, with crystallite size. The changes in lattice constant became interesting as there is a definite contraction of lattice seen with decreasing crystallite size. For nanoparticles unlike bulk solid as particle size decreases, surface-to-volume ratio increases. The resulting decrease in lattice constant can be due to strain induced by the increasing number of surface atoms in an effort to minimize the free energy of the surface. It is seen that the growth of grains has been occurred in the sintered sample, but not in other two annealed samples.

In a recent study Buscarino *et al.*[7] showed that sintering for a long time (~75 h) moulds the microscopic structure of silica nanoparticles to that of bulk materials. For the present study, the sample has been sintered for only 3 h and crystallites remained in nanophase but only increasing the size to 55.4 cm. This crystal growth in turn decreased the surface-to-volume ratio which caused the lattice constant to increase by reducing the surface free energy. The study of Diehm *et al.*[8] also supports this conclusion that surface tension plays a crucial role in determining lattice constant of metal oxide nanoparticles.

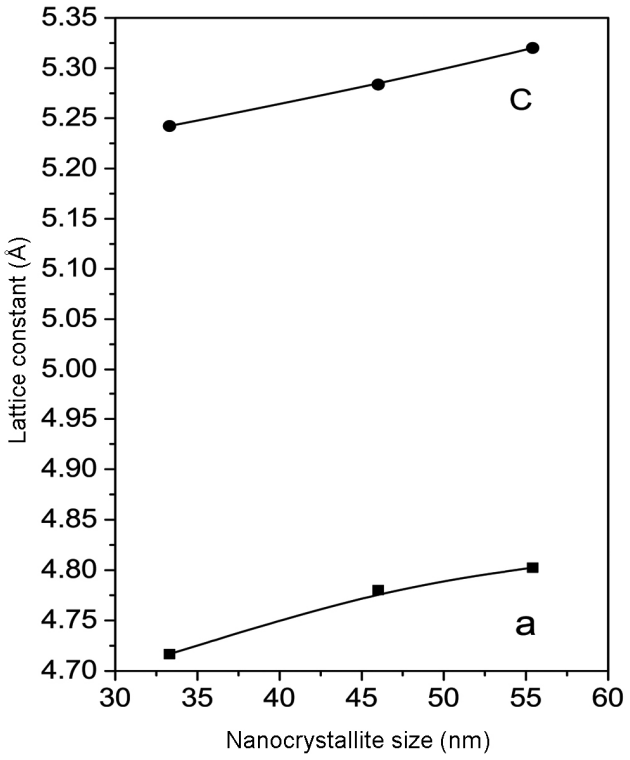

Figure 2. Variation of lattice constant (a, Å) with the nanocrystallite size of the samples.

HRTEM studies

Figure 3 displays HRTEM images of some SiO_2 samples. Figure 3 *a* and *b* shows samples entirely consisting of SiO_2 crystallites of size about 46 nm, larger particles or agglomerates being mostly absent. The figure also shows the spherical shape of the crystallites. Figure 3 *c* and *d* shows the densification of nanoparticles on sintering in air. The microstructure did not show much alteration as the sintering time was not long enough. Sintering made the nanoparticles dense by embedding smaller nanoparticles on larger nanoparticles.

UV–Vis measurements

UV–Vis light absorption spectroscopy is considered as an important method to determine the energy band structures and optical absorption properties of semiconductors. Figure 4 show optical absorption, i.e. UV–Vis spectra in the wavelength range from 190 to 650 nm for the annealed and sintered nanocrystalline samples. Evidently the absorption gradually decreases with increase in wavelength in the region from 190 to 650 nm. The figure shows shifting of absorption edge to the lower wavelength region with increase of nanocrystallite size. The optical band gap (E_g) is calculated from Tauc's relation: $\alpha h\nu = A(h\nu - E_g)^n$, where A is a constant, $h\nu$ the energy of the photon and the value of n is dependent on the nature of transition[9]. n is taken as 1/2 and 2 for direct and indirect transitions respectively. SiO_2 in its bulk state is an insulator. Rahman *et al.*[10] have shown that SiO_2 nanoparticles can exhibit different electronic transition characteristics and they are direct wide band gap semiconductors. To obtain the optical band gap for the samples, the linear portion of the $(\alpha h\nu)^2$ versus $h\nu$ curve was extrapolated to 0 on the y-axis. The band gap was in the range 5.91–5.83 eV. The gradual red shift of the absorption edge in the spectrum selected with decreasing crystallite size, ensures the lowering of band gap value (Figure 5). Figure 5 shows that the band gap is red-shifted which can be explained as different defects are present at the silica surface[1] due to incomplete formation of Si–O–Si tetrahedral network such as oxygen and silicon vacancies. On the surface of SiO_2 nanoparticles, there exists paramagnetic oxygen vacancies (≡Si···Si≡) with positive charge, or neutral dangling Si bonds (≡Si·)[10]. The stability of these centres increases linearly with increase in particle size and higher energy is required to excite the electrons.

Positron lifetime measurements

In Figure 6, the lifetime spectra of positrons for all the samples have been peak – normalized and plotted. Nature of the spectra is multi-exponential and slopes are

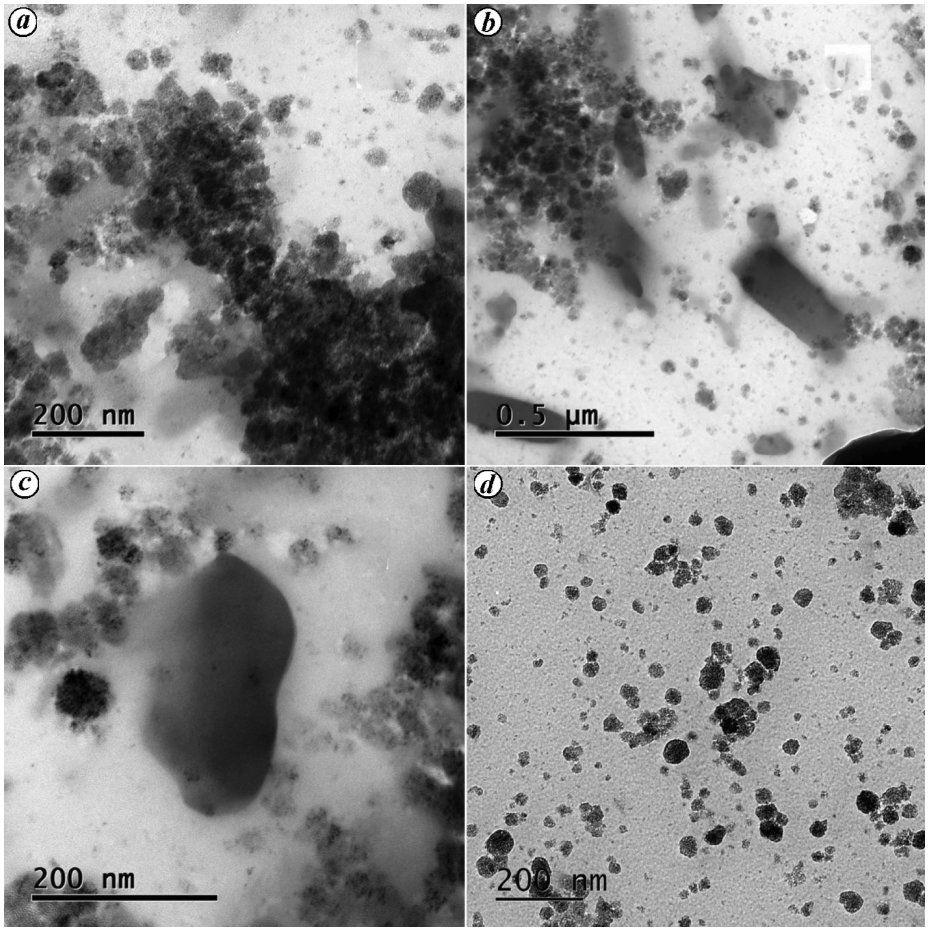

Figure 3. ***a–d***, HRTEM images of the samples. ***b***, ***c***, HRTEM images showing the sintered nanoparticles.

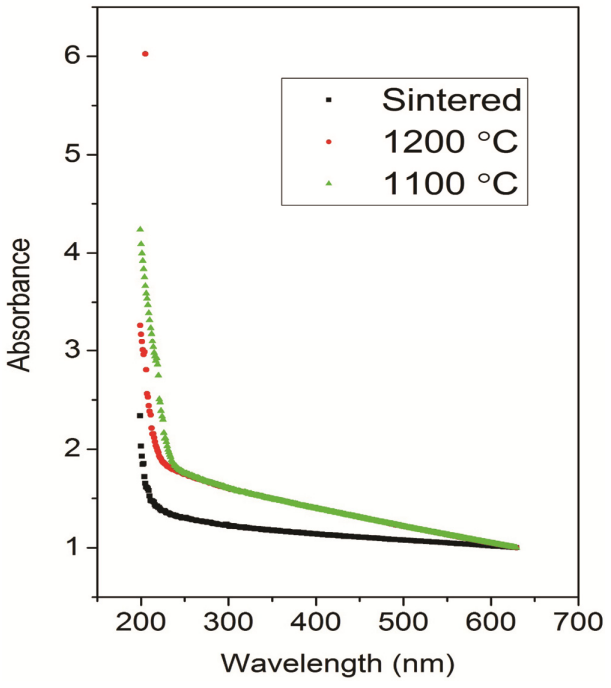

Figure 4. (Colour online) UV–Vis absorption spectra of the samples.

shallow, which signifies the presence of defects in high concentration in the samples prepared. All the positron lifetime spectra have been best-fitted using the program PALSfit with three lifetime components: τ_1, τ_2 and τ_3 in the ascending order of their magnitudes and their intensities in per cent are denoted as I_1, I_2 and I_3 respectively. Figure 7 *a* and *b* shows the lifetimes and intensities versus the nanocrystallite sizes. It is assumed that positron trapping rate for one kind of defect is proportional to its concentration, i.e. number of defects per unit volume. Obviously when defect concentration changes, the intensity of lifetimes also changes. From the rates with which the defects trap positrons, defect concentrations can be derived. Values of lifetimes are fairly large, which shows that defects are significantly larger in size and their concentrations are also equally large as indicated by the corresponding intensities on sintering. The longest lifetime τ_3, with intensity I_3, comes from the formation and annihilation of orthopositronium (o-Ps), which is a metastable bound state of the electron and positron (triplet spin) and parapositronium atoms (singlet state called parapositronium (p-Ps); here the spins of positron and electron are oriented opposite) that generally takes place

in sites where electron density is very low. It must be mentioned that for SiO_2 the thermal diffusion length of positrons has been reported as 10 nm (ref. 11) and the sizes of crystallites of the samples are greater than thermal diffusion length (Table 1). In other words, the annihilation probability of positrons at the nanocrystallite surface is negligible. The large percentage of (I_3 = 36.57–49.62%) orthopositronium and parapositronium bound states is therefore likely to be formed in the larger-sized defects, known as free volume cavities or holes. Their concentration is also equally high, which shows the high porosity of the samples. The values of τ_3 varied between 1.5 and 1.58 ns. Orthopositronium atoms undergo decay through the 'pickoff' process[12], with typical lifetimes of the order that we received. Positron is captured in o-Ps state by an electron with opposite spin from the material and consequently it annihilates. Jan *et al.*[13] showed a very slow thermalization process of o-Ps in SiO_2 and indicated the increase in orthopositronium lifetime which has occurred here also. From established Tau–Eldrup model, the values of τ_3 correspond to interfacial defects whose sizes are of the order of 0.56–0.61 nm. From this, it is implied that the particle separation is of this order and the powdered samples are well-separated which decreases with increase of crystallite size.

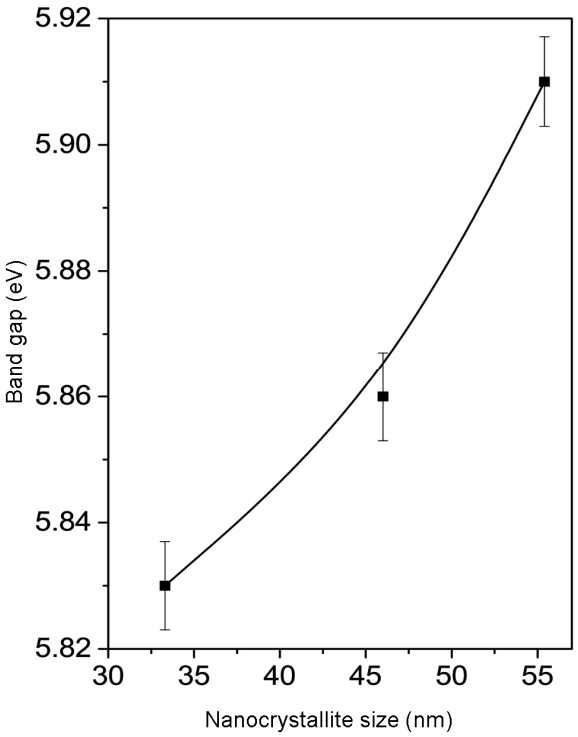

Figure 5. Bandgap versus size of the nanocrystallites of the samples.

Table 1. Annealing temperature and nanocrystallite size of the synthesized samples

Annealing temperature (°C)	Time (h)	Nanocrystallite size (nm)
1100	3	33.3
1200	3	46
1100 (sintering temperature)	3	55.4

The positron lifetime spectra are very long-lived and indicate the presence of defects in the solids. Figure 6 displays a marked distinction of the sample after annealing at 1200°C, showing considerable reduction of the positron lifetime and hence the formation of higher electron density regions. We obtained shorter lifetime τ_1 from free electron and positron annihilation and it varied between 120.5 and 144.4 ps. These lifetimes are below the bulk SiO_2 lifetime, τ_b varying reported[14] as τ_b = 186 to 266 ps. As the intensity of lifetime τ_3 is much greater due to o-Ps and p-Ps, the contribution probability of free electrons to τ_1 is very less. The values of intensity I_1 are not low. Free electrons from the trapped air in pores can annihilate with positrons and may have contributed to I_1. It can be said that as τ_1 of the unsintered smallest crystallize sized sample is largest, the number of free electrons inside the pores is least.

The intermediate lifetime τ_2 is defect-specific and varies for higher order vacancy-type defects depending on structure[15] and morphology. To understand it further, we first calculated a 'bulk' positron lifetime (τ_b) in SiO_2 using the relation

$$\frac{1}{\tau_b} = \frac{I_1}{\tau_1} + \frac{I_2}{\tau_2} + \frac{I_3}{\tau_3}. \quad (3)$$

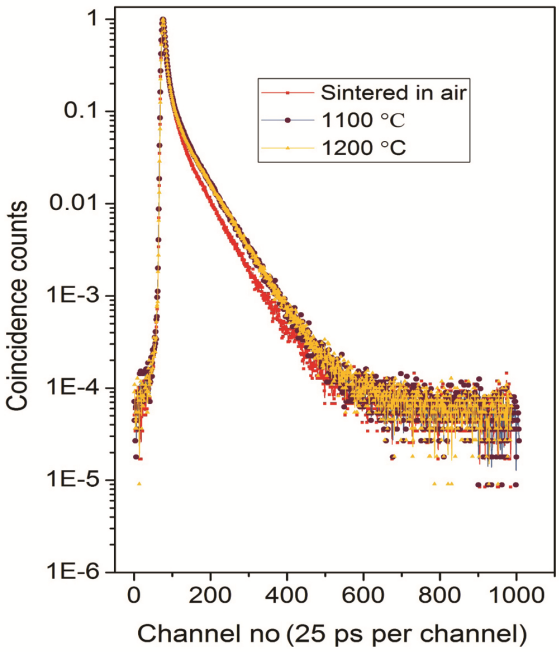

Figure 6. (Colour online) Peak-normalized positron lifetime spectra, i.e. coincidence counts versus channel number of the nanocrystalline samples.

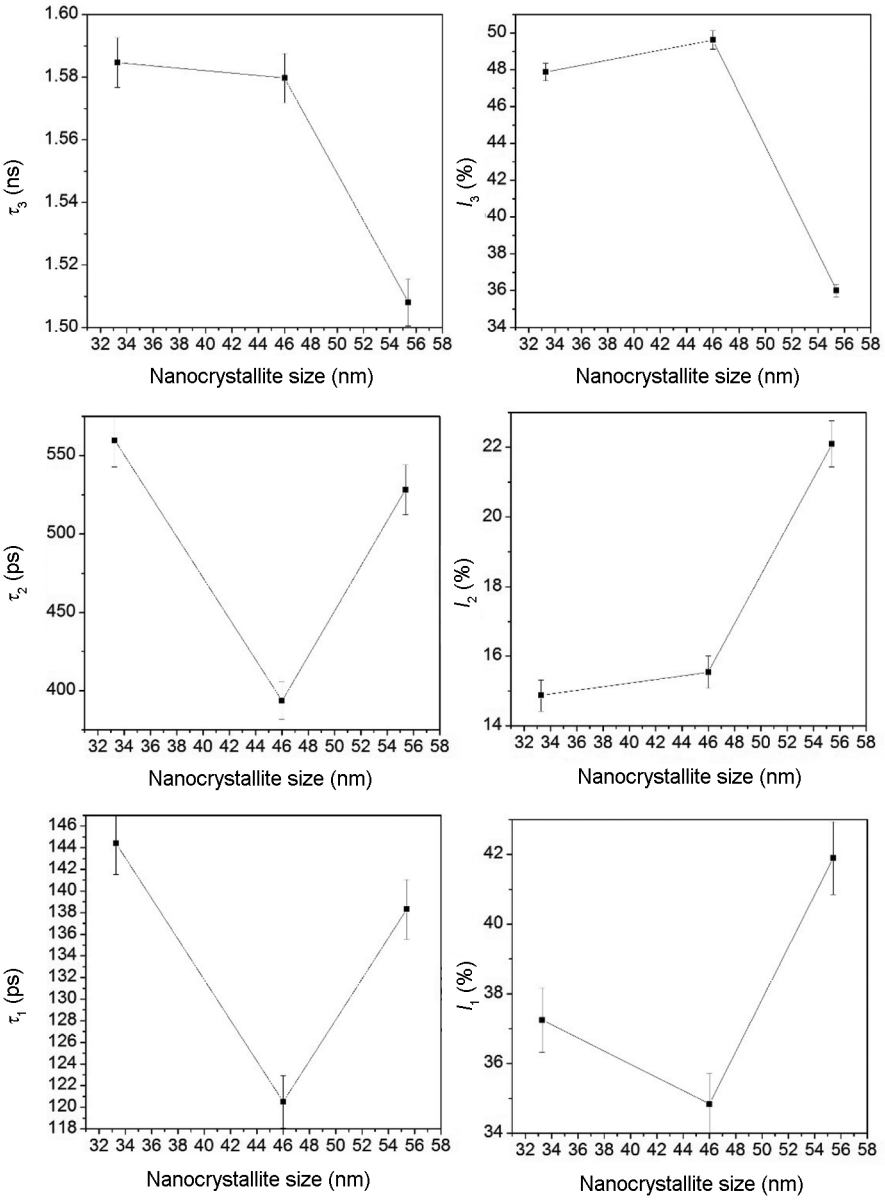

Figure 7. Variation in the positron lifetimes and percentage intensities versus size of the nanocrystallites of the samples.

The bulk lifetime so calculated has fallen from 303.9 to 271.2 ps due to sintering, a favourable indication of the formation of zones of increased electron density inside the nanocrystallites after sintering. This value is almost the same as reported for positron lifetime $\tau_b = 266$ ps in bulk SiO_2 (ref. 13) and hence the simple two-state trapping model based on which eq. (3) has been derived holds good in this context. Though the samples are nanocrystalline, as the size of crystallites is large enough than the thermal diffusion length (10 nm)[11], the positrons thermally diffuse inside the grains and do not get enough time to annihilate on the surface. So the positrons are trapped inside the crystallites and get annihilated therein. τ_2 has fallen from 560 to 393.7 ps on heating from 1100°C to 1200°C and again increased to 528 ps on sintering in air at 1100°C. This indicates that the size of the crystalline defects within the material grains has become intermediate on sintering. In other words, sintering at the same temperature reduces the defect sizes but increases nanocrystallite size, and this fact can be of much significance for material processing using SiO_2. The magnitudes of τ_2 are indeed very large and these lifetimes can correspond to void-like defects. Also, it is very likely that coalescence or defect agglomeration has occurred in the sintered sample. Comparison between the two heat-treated samples shows another behaviour of vacancy-type defects. The intermediate lifetime τ_2 has been decreased keeping the intensities more or less the same on increasing

the temperature. This indicates reduction in size of vacancy-type defects though concentration remained almost the same. So sintering and alteration of annealing temperature have opposite effect on vacancy-type defects that is readily seen by PAS.

When interior of the grains are decorated by larger cavities, which are called free volume defects, they can offer an environment for positrons favourable to form positronium with the electrons. When positrons are trapped inside those free volume defects, the positron and electron wave-function overlap probability is small. The positrons can stay there for a longer time and get annihilated. From the magnitude of τ_3, the free volume radius can be calculated using the Tao–Eldrup equation

$$\tau_3 = 0.5\left[1 - \frac{R}{R_0} + \frac{1}{2\pi}\sin\left(2\pi\frac{R}{R_0}\right)\right]^{-1}, \quad (4)$$

where the unit of τ_3 is in nanoseconds and R, R_0 are in Å. R_0 is an empirical parameter whose value is taken as 1.66 Å. Table 2 shows the results of this estimation. From the result it is evident that free volume radius has greatly shrunk after sintering. From lattice constant study (Figure 2) we found that surface-to-volume ratio had decreased. But surface has been increased as nanocrystallites become largest after sintering. So volume must have increased so much that the surface to volume ratio as ultimately decreased. It establishes that free volume defects has been reduced in radius as well as in concentration. The microstructural change in defect characteristics has been directly reflected in positron annihilation lifetime parameter I_3 that has been greatly reduced from 47% to 36%, which proves the reduction in concentration of free volume defects. PAS can be used as a probe to the change in microstructure at atomic levels as well.

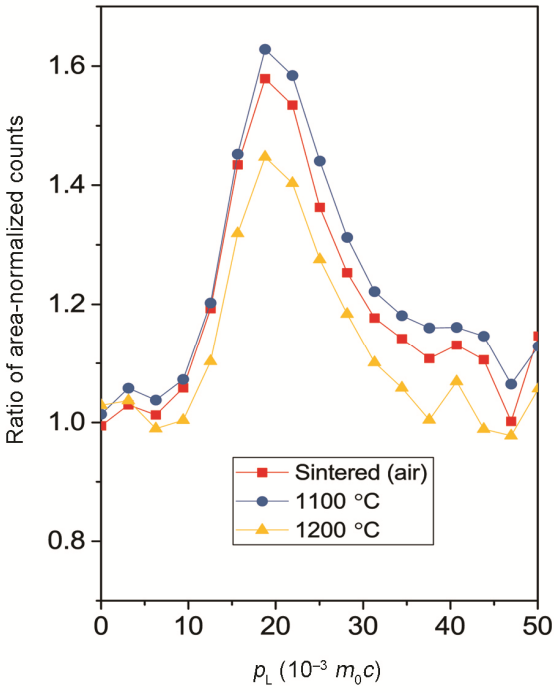

Figure 8. (Colour online) CDBS ratio curves of samples with reference to the spectrum of well-annealed Al pellets.

Table 2. Free volume hole radius in the samples calculated from the Tao–Eldrup equation

Sample information	τ_3 (ns)	Free volume radius R(Å)
Sintered in air	1.5080	2.35
1100°C	1.5846	2.44
1200°C	1.5797	2.43

Coincidence Doppler broadening measurements

The CDBS measurements were carried out by conventional method[16]. The one-dimensional projection is on the energy-difference axis and integrated over 1.022 ± 0.0024 MeV. Electron momentum distributions within the samples as seen by the annihilating positrons[17] are different, but the differences are too small to make any visual conclusions. Hence a normal procedure to overcome these differences is to make ratio curves by dividing these

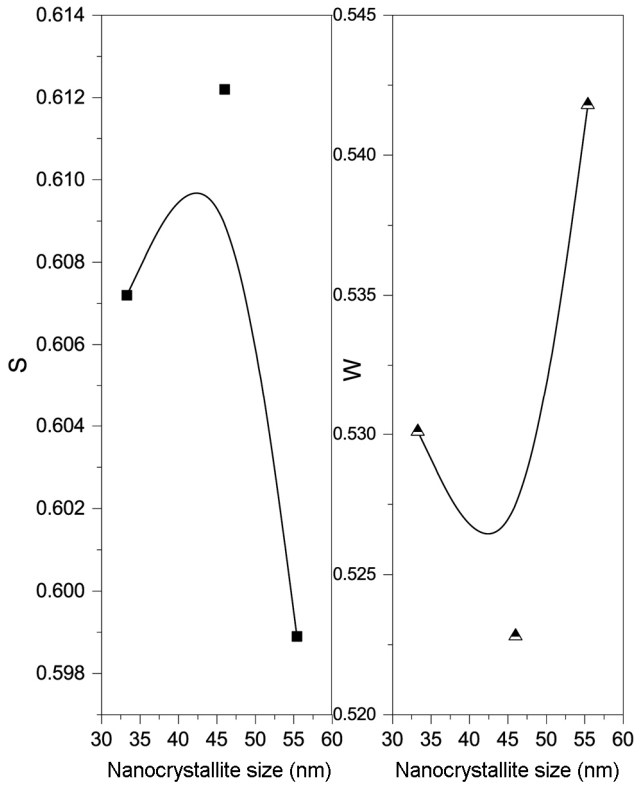

Figure 9. *S* sand *W* parameters versus size of the nanocrystallites of the samples.

spectra by an identically obtained and area-normalized spectrum of a reference sample, pure (99.999%) and annealed (at 625°C for 2 h in vacuum $p \sim 10^{-6}$ mbar) single crystalline aluminium in this case. Figure 8 shows the obtained results. A characteristic peak seen around the electron momentum $p_L = 20 \times 10^{-3}\ m_0c$ is coming from the O^{2-} core electrons. Area under the central part of the curve signifies the total low momentum contribution and the region for high momentum contribution is far from the centre. The peak becomes sharper for the annihilation with 2p electrons than 2s electrons of the surrounding chemical environment. The peak is sharper for the sintered sample, indicating that proximity to the 2p oxygen electrons is more in the sintered sample. This result also supports the previous finding of shrinkage of free volume radius after sintering. The decreased peak height in ratio curve for 1200°C supports the earlier findings of removal of defects as annealing temperature increases. More insight into the CDBS data reveals some interesting facts about defect characteristics of sintered sample. The Doppler broadened electron–positron annihilation γ-ray spectrum is analysed in terms of the so-called line-shape parameter S and wings parameter W (Figure 9). The S-parameter is calculated from its definition – the ratio of the counts under central area of the 511 keV photo peak to the total counts under the whole spectrum. The S-parameter represents the fraction of positrons annihilating with the electrons of low momentum with respect to the total number of annihilated electrons. The W-parameter is the relative fraction of the counts in the wing regions of the annihilation spectrum with that under the whole spectrum. The W-parameter is taken from the annihilation events of positrons with the high momentum electrons. Here the S-parameter for the sintered sample is less than that for the unsintered but calcined at 1100°C and 1200°C samples. As free volume defect size and concentration have reduced in sintered sample, the fraction of low momentum electrons annihilating with trapped positrons is in line with lineshape parameter. Coming to the straight line nature of S–W plot in Figure 10, we recall that during synthesis of the samples, the annealing temperature has been increased by a step of 100°C. The increase of temperature forces the vacancy-type defects to agglomerate. From the S–W plot, it is clear that the clusters of defects where the positrons are trapped basically remain of the same configuration and origin. Any other positron trapping defects were not found in the samples such as dislocations and loops.

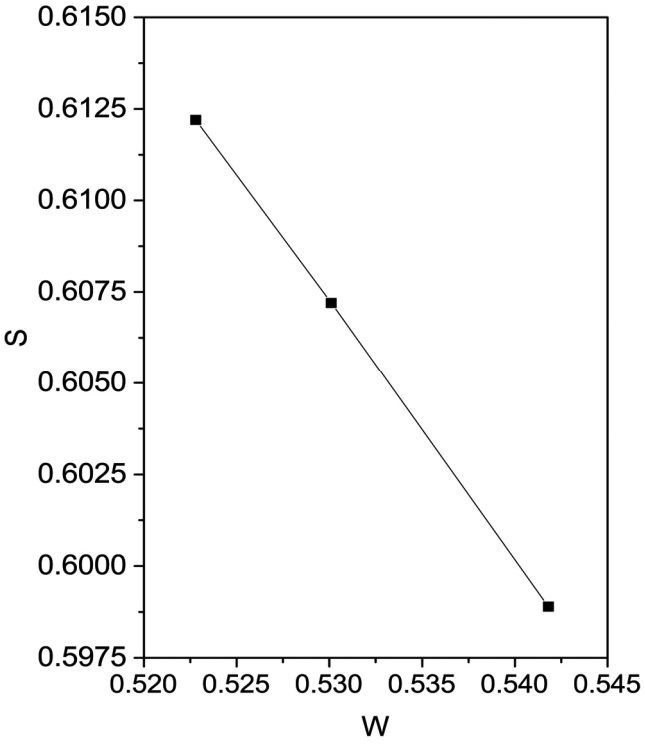

Figure 10. S–W plot.

Summary and conclusion

From the point of view of synthesis, it should be mentioned that the sol–gel process successfully produced samples in sufficient degree of purity and narrow distribution of size in the nanometre range 33.3–55.4 nm. Subsequent study on their structure revealed the crystallite size and lattice contraction with decreasing crystallite size. HRTEM showed the nearly spherical shape of the particles. UV–Vis spectroscopy clearly showed red shift of the absorption edge. It also revealed oxygen or both silicon and oxygen vacancies on the surface of nanoparticles. Here PAS results also resemble the findings of lattice constant change as there has been a remarkable reduction in the positron lifetime intensity I_3. The shortest lifetime τ_1 indicated that sintering increases the free electron density in SiO_2. The intermediate lifetime τ_2 indicated the presence and shrinkage of free volume defects as temperature increases. Also, from large values of τ_2 and I_2 it can be mentioned that large defects with increased concentration from bulk value are present and concentration increases with higher temperature as also with sintering. The study assumes significance as a demonstration of sintering as a tool for reduction of vacancy defects with reliability of PAS for such studies.

1. Rahman Ismail, A. and Padavettan, V., Synthesis of silica nanoparticles by sol–gel: size-dependent properties, surface modification, and applications in silica–polymer nanocomposites – a review. *J. Nanomater.*, 2012, **2012**, 1–15.
2. Rajendran, J., Hamid, S. S., Mohd, S. K. K., Abdullah, M. Z., Ramiah, H. and Kumar, N., An integrated linearization technique for GaAs bipolar WCDMA power amplifier. *Curr. Sci.*, 2018, **114**(2), 308–313.
3. Hassan, E. M., Characterization of control mesoporous glasses (CPGs) using positron annihilation lifetime spectroscopy (PALS), Ph D thesis, Martin Luther University, Halle-Wittenberg, 2007.

4. Olsen, J. V., Kirkegaard, P., Pedersen, N. J. and Eldrup, M., PALSfit: a new program for the evaluation of positron lifetime spectra. *Phys. Status Solidi C*, 2007, **4**, 4004–4006.
5. Chatterjee, A., Ramachandran, K., Kumar, A. and Behere, A., Linux Advanced MultiParameter System. Trombay, Mumbai; http://www.tifr.res.in/~pell/lamps.html (accessed on July 2015).
6. Cullity, B. D., *Elements of X-ray Diffraction*, Addison-Wesley, Massachusetts, USA, 1956.
7. Buscarino, G., Ardizzone, V., Vaccaro, G. and Gelardi, F. M., Sintering process of amorphous SiO_2 nanoparticles investigated by AFM, IR and Raman techniques. *J. Non-Crystalline Solids*, 2011, **357**, 1866–1870.
8. Diehm P. M., Agoston, P. and Albe, K., Size-dependent lattice expansion in nanoparticles: reality or anomaly? *ChemPhysChem*, 2012, **13**, 2443–2454.
9. Dutta, S., Chattopadhyay, S., Sarkar, A., Chakrabarti, M., Sanyal, D. and Jana, D., Role of defects in tailoring structural, electrical and optical properties of ZnO. *Prog. Mater. Sci.*, 2009, **54**, 89–95.
10. Rahman, I. A., Vejayakumaran, P., Sipaut, C. S., Ismail, J. and Chee, C. K., Size-dependent physicochemical and optical properties of silica nanoparticles. *Mater. Chem. Phys.*, 2009, **114**, 328–332.
11. Ghislottia, G., Nielsen, B., Asoka-Kumar, P., Lynn, K. G., Di Mauro, L. F., Corni, F. and Tonini, R., Positron annihilation studies of silicon-rich SiO_2 produced by high dose ion implantation. *Appl. Phys. Lett.*, 1997, **70**(4), 496–498.
12. Siegel, R. W., Positron annihilation spectroscopy. *Ann. Rev. Mater. Sci.*, 1980, **10**, 393–425.
13. Jan, W., Jacek, G., Radoslaw, Z. and Tomasz, G., Positron lifetime in mesoporous silica of MCM-41 type. *Langmuir*, 2003, **19**(7), 2599–2605.
14. Kuriplach, J. and Barbiellini, B., Gradient correction scheme for bulk and defect positron states in materials: new developments. *J. Physics: Conf. Ser.*, 2014, **505**, 012040–012048.
15. Rajesh, P., Sellaiyan, S., Uedono, A., Arun, T. and Joseyphus, R. J., Positron annihilation studies on chemically synthesized FeCo alloy. *Nature*, 2018, **8:9764**, 1–9.
16. Das, A., Mandal, A. C. and Nambissan, P. M. G., Effect of size on momentum distribution of electrons around vacancies in NiO nanoparticles. *Chin. Phys. B*, 2015, **24**(4), 046102–046104.
17. Amarendra, G., Viswanathan, B., Rao, V. G., Parimala, J. and Purniah, B., Variable low energy positron beams for depth resolved defect spectroscopy in thin film structures. *Curr. Sci.*, 1997, **73**(5), 409–417.

ACKNOWLEDGEMENTS. I thank Dr Goutam Das, National Metallurgical Laboratory, Jamshedpur, for help during data acquisition using XRD, HRTEM and UV–Vis spectroscopy. I also thank Dr P. M. G. Nambissan, Saha Institute of Nuclear Physics, Kolkata for help with positron annihilation spectroscopy.

Received 24 October 2018; revised accepted 20 August 2019

doi: 10.18520/cs/v117/i12/1990-1998